- Date written: 27.11.2020
- Number of words in main text 5895; number of tables 2, number of figures 10.

Numerical modelling of the resistance of the coarse sand barrier against backward erosion piping

Author 1

- Esther Rosenbrand, Dr. MSc.
- Unit Geo-Engineering, Deltares, Delft, The Netherlands
- https://orcid.org/0000-0001-9274-6229

Author 2

- Vera van Beek, Dr. MSc.
- Unit Geo-Engineering, Deltares, Delft, The Netherlands
- https://orcid.org/0000-0002-8765-3439

Author 3

- Adam Bezuijen, Professor
- Department of Civil Engineering, Ghent University, Ghent, Belgium
- Unit Geo-Engineering, Deltares, Delft, The Netherlands
- https://orcid.org/0000-0002-5591-0461

Corresponding author:

Esther Rosenbrand

Deltares

Boussinesqweg 1

2629 HV, Delft, the Netherlands

Email: esther.rosenbrand@deltares.nl

Tel: +31 88 3357852

Abstract

The coarse sand barrier (CSB) is a novel remediation measure to reinforce embankments against the internal erosion mechanism of backward erosion piping (BEP). The feasibility of the CSB is investigated in a research programme consisting of experiments at different scales, numerical analysis, and application at a pilot site in the Netherlands. Laboratory experiments showed that the CSB increased the critical head drop for BEP by one order of magnitude. In this paper, the strength of the CSB is quantified using numerical modelling of the experiments. A local, scale-independent, strength criterion for the CSB is derived based on medium-scale experiments. The application of this local criterion is illustrated for a field scale model, in which the critical head drop that can be retained increases by a factor two to three with the CSB.

Keywords chosen from ICE Publishing list

Erosion; Remediation; Embankments, numerical modelling

List of notations

COV	coefficient of variation, the ratio SD/μ, -
C_u	uniformity coefficient, the ratio d_{60}/d_{10}, -
h_{cp}	effective head drop at the critical time instant for pipe progression, m
i_{cp}	local critical hydraulic gradient for primary erosion at the pipe tip, -
$i_{cp,exp}$	measured secant gradient in the barrier at the critical time instant (t_c), -
$i_{cp,num}$	strength criterion, critical secant gradient in the barrier for numerical modelling, -
t_c	critical time instant for pipe progression, s
K	hydraulic conductivity, m/s
RD	relative density based on void ratio $(e_{max}-e)/(e_{max}-e_{min})$, -
SD	standard deviation, -
μ	mean, -

1. Introduction

Rising sea levels, in combination with the increase of both population and economic value in flood prone areas, increase the demand for adequate flood defences (Winsemius et al., 2016). The failure mechanism of backward erosion piping (BEP) poses a threat to flooding along embankments; breaches attributed to BEP were reported in the Netherlands (Vrijling et al., 2010), the United States (Navin, 2016) and China (Yao et al., 2009). BEP threatens embankments founded on a granular aquifer overlain by a cohesive blanket. It is driven by the hydraulic head drop across the aquifer, which causes seepage and can transport grains out of the aquifer's unfiltered exit. This results in a sand boil at the surface, and formation of small hollow pipes in the aquifer below the blanket. One or more pipes develop predominantly in the upstream direction if the high-water level persists (Figure 1), and can progress below the embankment to cause a hydraulic shortcut with the outer water body. At this point, erosion increases dramatically, causing settlement and deformation of the levee or embankment and ultimately flooding (van Beek et al., 2011).

The rising risk associated with flooding calls for novel remediation measures, as existing solutions such as sheet pile walls, seepage berms, or drainage are respectively expensive, unpopular in densely populated areas, or require maintenance. Therefore, the coarse sand barrier, CSB, is investigated as a nature based, sustainable and cost-effective solution. The CSB consists of a trench dug below the embankment toe, that is filled with densified coarse sand or gravel and prevents the pipe from progressing upstream (Figure 1). As opposed to a drainage measure, the CSB will only act once a pipe has already formed. This means that during normal operation there is little to no risk of clogging.

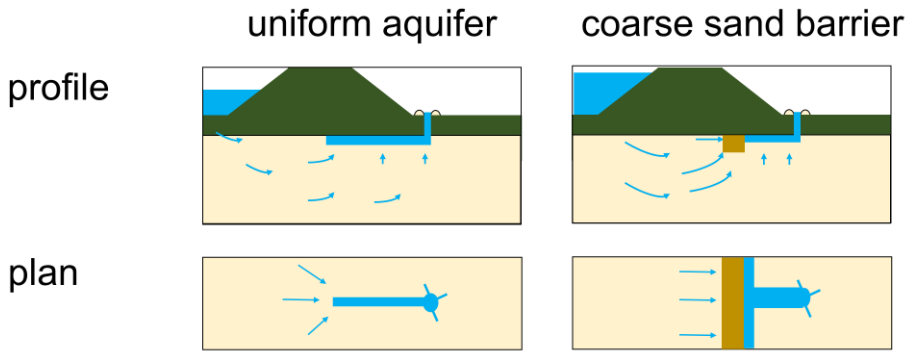

Figure 1: Concept of the CSB (not to scale). L.h.s. backward erosion piping without a barrier a pipe can progress upstream below the embankment, r.h.s. the pipe is stopped by the CSB (modified after Rosenbrand et al., 2020).

The effectiveness of the CSB is based on the theoretical understanding of pipe progression, which is considered to be governed by: a) primary erosion, the loosening of grains at the pipe tip driven by the hydraulic gradient at the pipe tip, and b) secondary erosion, transport of grains in the pipe (e.g., Hanses, 1985; van Beek et al., 2015; Robbins et al., 2018). A well-designed CSB fulfils the filter rules, and affects primary erosion in two ways: 1. the higher permeability of the CSB as compared to the background sand reduces the hydraulic gradient in the barrier; 2. a well sorted barrier with a high relative density (*RD*) has a higher resistance to erosion (Rosenbrand et al., 2020). Therefore, a pipe which encounters the barrier is prevented from progressing upstream and will rather grow parallel to the barrier in the background sand, seeking the weakest path (Figure 1). This has the added benefit that it reduces the concentration of flow in the barrier, further reducing the hydraulic gradient in the barrier (Negrinelli et al., 2016; Rosenbrand et al., 2018).

In order to use a CSB as a reinforcement measure, it's strength must be quantified, and a design approach is required to predict the water level that can be retained. The hypothesis is that resistance of a barrier against primary erosion can be characterised by a critical hydraulic gradient at the pipe tip, i_{cp}. The i_{cp} is expected to be a material property, which depends on sorting (characterised by the coefficient of uniformity, C_u) and relative density (*RD)* (e.g.

Robbins et al., 2018; Schmertmann et al., 2000; Rosenbrand et al., 2020). As i_{cp} is expected to be independent of scale, barrier dimensions, or properties of the background sand, a strength criterion $i_{cp,num}$ based on i_{cp} could be used in numerical modelling to predict the strength of a barrier for any configuration. As the head profile at the pipe tip is nonlinear due to converging flow to the pipe, the question is over which distance, and in which direction, the gradient is representative for the process. Although Discrete Element Models (DEM) can be used to resolve physical processes on a grain scale (e.g. El Shamy & Aydin, 2008; Froiio et al., 2019) these are computationally expensive. Horizontal secant gradients over 0.10 m upstream of the pipe tip, appeared suitable to characterise i_{cp} in BEP experiments on homogeneous sands (Robbins et al., 2018). Gradients over this scale can be analysed using Finite Element Models (FEM), which can also be applied on the field scale.

The characterisation of $i_{cp,num}$ is addressed in the current paper, which is part of a feasibility study to investigate the potential of a CSB. The feasibility study consists of experiments at three scales followed by application at a pilot location in the Netherlands. Small-scale tests were used as a proof of concept, the medium-scale tests are used to test the concept and quantify a strength criterion, and the large-scale tests were intended to serve as a verification. Experiments at all scales are presented and analysed in Rosenbrand et al. (2020). The experiments showed that the barrier provides a significant strength gain in terms of the total head drop that can be retained. Pore water pressure measurements inside the barrier suggested that the critical gradient inside the barrier, $i_{cp,exp}$ is indeed a suitable indicator of barrier strength. As the gradients were measured over a fixed distance and not exactly at the pipe tip, numerical modelling is required to confirm this. The medium-scale tests were used for modelling a strength criterion as the CSB is too thin in the small-scale tests, and in the large-scale tests the number of unknown variables was too large (Rosenbrand and van Beek, in press). The large-scale test did reveal that 3D effects might play a role, which is relevant as a 2D modelling approach is envisaged for design.

The current paper presents the modelling of the medium-scale tests, and the selection of a strength criterion that characterises the resistance of the CSB against erosion, $i_{cp,num}$. The conclusions and implications of modelling the large-scale experiment are briefly discussed.

Finally, a prediction method for modelling the strength of the CSB on a field scale is presented and used to illustrate the effect of the CSB on the critical head drop that can be retained.

2. Experiments

A summary of the experiments is provided to support the modelling strategy, details are provided in Rosenbrand et al. (2020). Small- and medium-scale experiments were performed in a rectangular set-up with a transparent acrylate cover, so that pipe progression could be observed. Sample dimensions (l×w×d) are 0.480×0.300×0.100 m for small, and 1.910×0.881×0.404 m for medium scale tests. The large-scale tests were performed by building an aquifer (3 m deep, 5 m wide, seepage length 15 m) covered by a cohesive clay blanket in the Delta Flume facility of Deltares. For all tests, the barrier was placed directly underneath the cover, perpendicular to the flow direction, along the entire width of the set-up. The barrier was 0.3 m thick in most medium-scale tests and in the large-scale tests. The barrier depth was varied in medium-scale tests and was 0.5 m in the large-scale tests. Pore pressure transducers (PPT) were installed at the top and at the bottom of the set-ups. Flow entered through a filter along the entire upstream end of the box for small- and medium-scale tests and left through a hole in the top of the acrylate cover. For the large-scale tests, the aquifer surface was in contact with the upstream water body, and flow exited through a ditch dug parallel to the flow direction (in order to concentrate flow to the centre of the set-up). The head drop was increased stepwise. Plan views of the samples and locations of pore pressure transducers are included in S1.

The piping process was followed based on visual observations and measurements for the small- and medium-scale tests. One or more pipes formed at the outlet hole and progressed predominantly in the upstream direction up to the barrier. With increasing head drop, the pipe progressed parallel to the barrier interface, along the width of the set-up. Some barrier grains rolled into the pipe (crumbling), and some short (a few centimetres) pipes formed at the edge of the barrier along the width of the set-up. These came to a halt, and further head increments were required for the pipe to lengthen further. In medium-scale tests, one head increment caused a significant progression of the pipe, which reduced the hydraulic heads in the barrier and upstream. This step could be observed visually and in pore pressure measurements, and is considered as the critical step to characterise the barrier strength, referred to as the progression

step. The barrier was too thin in small-scale tests to determine this step. In some cases, the progression step also led to the pipe breaching through the upstream interface of the barrier, causing failure. In one large scale experiment, due to the test configuration a different failure mechanism occurred, therefore only the other large-scale experiment is analysed in this paper. As the cover in large-scale experiments was a cohesive clay blanket, the progression step was deduced from pore water pressure measurements. Pore water pressure measurements indicated that the pipe only progressed a limited distance parallel to the barrier prior to the progression step, possibly due to a relatively fast rate of applying the load in this experiment. The time interval, t_c, preceding the progression step, is the last stable situation prior to the progression step and thus the critical time instant for progression. The pore pressures at the critical time instant are modelled in order to determine a strength criterion for a CSB.

3. Modelling the medium-scale experiments

The objective of the models is to determine the head profile in the barrier at t_c and define the length over which the critical secant gradient is suitable as a strength criterion, $i_{cp,num}$. For design, it is highly desirable to use 2D models (cross section of the embankment). Progression of the pipe parallel to the barrier, results in an effectively 2D flow field inside the barrier (Negrinelli et al., 2016; Rosenbrand et al., 2018), therefore 2D models are used to analyse the medium-scale tests.

The pipe is modelled as a constant head boundary condition along the upper boundary of the flow domain (Figure 2), running from the outlet hole to the furthers point that crumbling or short pipes had formed inside the barrier. The head loss in the pipe is assumed to be negligible, which is supported by measurements (Rosenbrand et al., 2020). The flow field is predominantly 2D due to the pipe forming parallel to the barrier along the entire model. The presence of a short pipe inside the barrier does introduce a 3D component, due to convergence of flow to the pipe tip. However, as typically multiple short pipes are inside the barrier, the 2D models are considered appropriate. For the large-scale test, where the pipe did not progress parallel to the barrier interface along the entire set-up, 2D models were less appropriate (Rosenbrand and van Beek, in press), as discussed at the end of this chapter. This Chapter describes the models, and presents and analyses the main results, further data is available upon request.

3.1 Model description

Modelling is done using the finite element groundwater model DgFlow (van Esch et al., 2013) using first order elements. Steady state flow is modelled using the Darcy equation. The mesh has 0.001 m quadrilateral elements inside the barrier; the element size increases gradually to 0.005 m at the upstream and downstream sides. A higher level of mesh refinement did not significantly affect the computed strength criterion (Rosenbrand et al., 2018).

The inlet and the outlet are modelled as constant head boundary conditions (Figure 2), other boundaries are closed. The pipe length, the upstream head and the head in the pipe are based on measurements and observations at t_c. The critical head drop h_{cp} is the head drop up from the upstream head boundary up to the pipe. Two models with a 0.30 m and with a 0.45 m thick barrier are shown in Figure 2.

a)

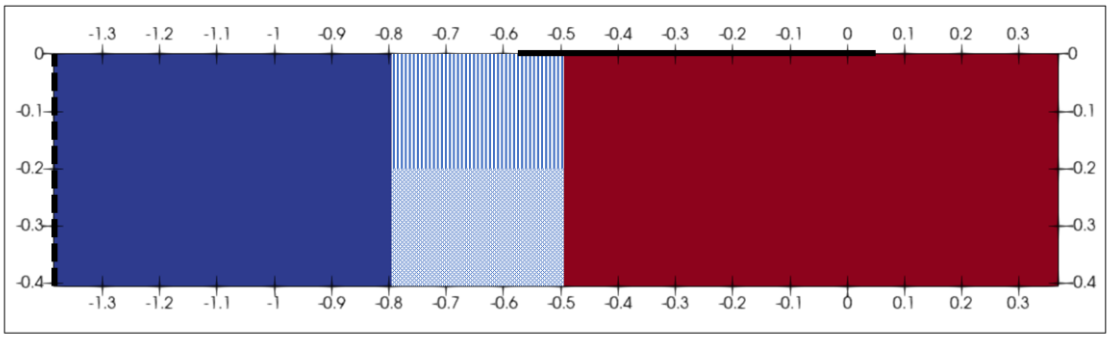

b)

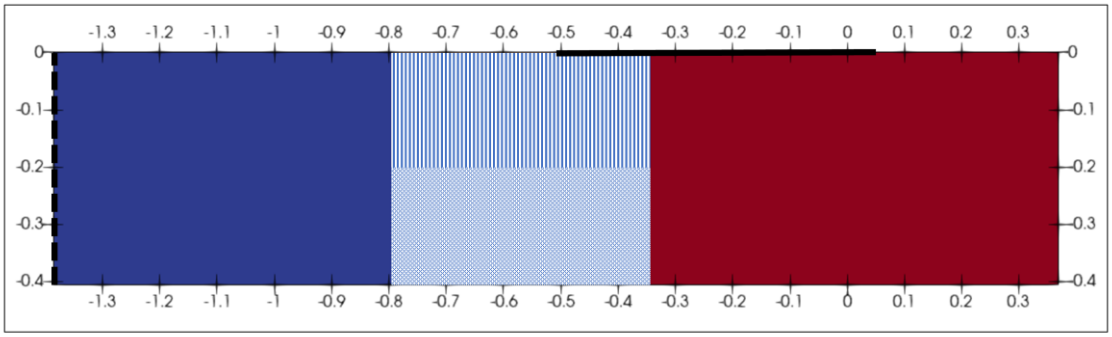

Figure 2. Models for barrier thickness 0.30 m (a) and 0.45 m (b). The barrier is the area with vertical lines, the other soil blocks consist of background sand with different RD. Flow is from left hand side (inlet =dashed black line) to right hand side (outlet is the pipe = solid black line). The pipe length inside the barrier at the critical time instant differs per model (Table 1).

The initial hydraulic conductivity, *K,* for the different layers is based on the correlation between *K* and *RD*, which was derived from column permeability experiments for these soils. There can be some difference between the *RD* of the background sand on the different sides of the barrier due to the method of preparation. The modelled *K* is adjusted in order to fit the head profile inside the barrier and match the flow rate measurement. An overview of the models and modelled hydraulic conductivities is shown in Table 1.

Table 1. Overview of numerical models.

	soil type		RD barrier	barrier dimensions		pipe length in barrier[+,**]	head drop[**]	Hydraulic conductivity m/s			
test	barrier [‡]	Back-ground[†]		depth, m	thick-ness, m	m	m	barrier	up-stream	down-stream	below
M23	GZB1	B15	0.81	0.40	0.30	0.06	3.48	1.3E-3	7.1E-5	8.0E-5	N/A
M24	GZB2	B25	1.04	0.40	0.30	0.12	1.06	9.3E-4	1.6E-4	2.1E-4	N/A
M25	GZB1	B25	1.01	0.125	0.30	0.06	1.91	1.5E-3	1.8E-4	2.1E-4	2.10E-04
M26	GZB1	B25	0.89	0.40	0.30	0.08	1.73	1.1E-3	1.6E-4	1.9E-4	N/A
M27	GZB1	B25	0.59	0.40	0.30	0.08	0.76	1.7E-3	3.0E-4	2.9E-4	N/A
M28	GZB2	MZ	0.85	0.40	0.30	0.04	0.61	1.3E-3	3.2E-4	3.6E-4	N/A
M29	GZB1	B25	0.91	0.125	0.30	0.04	1.12	1.4E-3	1.9E-4	2.1E-4	2.70E-04
M30	GZB1	B25	0.94	0.20	0.30	0.08	1.92	1.4E-3	1.7E-4	2.2E-4	2.70E-04
M31	GZB1	B25	0.87	0.20	0.45	0.15	1.94	1.5E-3	1.9E-4	2.4E-4	1.47E-04
M32	GZB1	B25	0.83	0.20	0.45	0.18	1.41	1.6E-3	1.9E-4	2.4E-4	2.08E-04
M33	GZB1	B25	0.85	0.40	0.30	0.11	1.76	1.3E-3	1.9E-4	2.1E-4	N/A
M34	GZB1	B15	1.06	0.20	0.30	0.04	3.61	1.4E-3	7.0E-5	7.4E-5	7.49E-05
M35	GZB5	B25	1.00	0.20	0.30	0.07	4.12	4.0E-3	2.1E-4	2.3E-4	2.93E-04
M36	GZB5	B25	0.85	0.20	0.30	0.07	5.52	5.1E-3	1.9E-4	2.4E-4	2.93E-04

‡ GZB1 mixture with d_{50} 1.402 mm, Cu 3.7, GZB2 mixture with d_{50} 0.870 mm, Cu 2.5; GZB5 mixture with d_{50} 2.259 mm, Cu 3.2

[†]MZ = Metselzand (d_{50} 0.377 mm, Cu 2.4), B15 = Baskarp 15 (d_{50} 0.151 mm, Cu 1.6), B25 = Baskarp 25 (d_{50} 0.228 mm, Cu 1.6)

[+] based on visual observation with an estimated uncertainty 0.02 m.

[**] at t_c.

3.2 Results and analysis

3.2.1 Assessment of the models

To assess how well the model approach, with the assumptions of 2D flow and no head loss in the pipe, represents the experiments, three aspects are assessed. The modelled head profile is compared to the measured heads in the pore pressure transducers that are placed in the sample just below the perspex plate at the top, and just above the bottom of the set-up (Figure 3). By making small adjustments to *K* for the soils in the models, a good fit was obtained, as shown in Figure 3. The fit inside the barrier is quantified by comparing the measured gradient in the barrier, $i_{cp,exp}$, to the modelled gradient over that same distance (Figure 3). The deviation is less than 5% for the experiments in which the pipe was present in the barrier below the downstream pore pressure transducer. In one experiment (M32), this was not the case, therefore the measured gradient $i_{cp,exp}$ does not reflect the gradient upstream of the pipe tip. This illustrates the need for the numerical models for determination of the strength criterion.

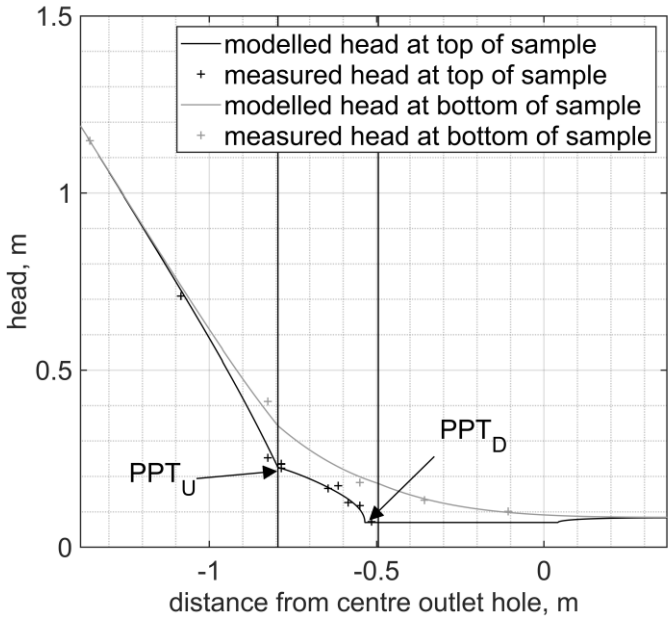

Figure 3: Modelled head profile (line) and measurements at the top (black) and bottom (grey) of the set-up for test M29. PPT_U (upstream in the barrier) and PPT_D (downstream) are used to calculate the measured gradient over the barrier $i_{cp,exp.}$

The ratio of the modelled *K* to the value that is expected based on *RD* serves as a second means of model evaluation (Table 2). The modelled ratios for the background sand upstream of the barrier are consistently higher than values based on *RD*, but the difference is small relative to the expected uncertainty for *RD* (uncertainty for *RD* is approximately 0.2).

The modelled ratios for the barrier show no consistent over- or underestimation, and match the expected values well, with two exceptions. Those are tests M25 and M34, for which the *RD* estimate based on preparation is higher than for other tests. For M34 thin bands of fine sand were observed in the barrier after preparation. Although these did not appear to affect the progression of the pipe in the barrier, these might also have affected the *RD* estimate. For M25 there was no obvious cause of the high *RD.* The hydraulic conductivity below and downstream of the barrier has relatively less effect on the modelled head profile. Due to the assumptions of no head loss in the pipe and 2D flow, larger deviations between models and reality would be expected downstream of the barrier.

The ratio of the modelled flow rate to the measured flow rate is a third means to assess the models, this ratio is between 1.00 and 1.04 for all models (Table 2).

196 Overall, these models provide a reasonable representation for modelling the head in the barrier
197 and upstream of the barrier. Therefore, this approach is considered appropriate to investigate
198 $i_{cp,num}$.

199 *Table 2. Numerical modelling results.*

test	Ratio hydraulic conductivity model over hydraulic conductivity based on preparation				Ratio modelled flow rate over measured flow rate	Horizontal secant gradient 10 cm upstream of pipe tip
	barrier	upstream	downstream	below		
M23	0.9	1.1	1.1	N/A	1.00	1.23
M24	0.9	1.1	1.2	N/A	1.03	0.82
M25	1.4	1.2	1.2	1.2	1.01	1.37
M26	0.9	1.1	1.1	N/A	1.03	1.27
M27	0.9	1.0	1.0	N/A	1.00	0.67
M28	1.0	1.1	1.0	N/A	1.04	0.76
M29	1.1	1.2	1.3	1.4	1.02	0.94
M30	1.2	1.0	1.2	1.3	1.01	1.26
M31	1.1	1.1	1.4	N/A	1.00	1.19
M32	1.2	1.1	1.2	1.2	1.03	0.82
M33	1.0	1.2	1.1	N/A	1.03	1.24
M34	1.5	1.0	1.1	1.0	1.02	1.32
M35	1.2	1.3	1.5	1.2	1.02	1.36
M36	1.2	1.2	1.2	1.1	1.01	1.32

200
201 *3.2.2 Head profiles*

202 To assess whether a local gradient upstream of the pipe is a good indicator of erosion
203 resistance, and whether this is indeed not affected by barrier dimensions or background sand
204 properties, the modelled head profiles along the top of the model are shown in Figure 4 for tests
205 with GZB1. A point of inflection occurs at the upstream end of the barrier due to the hydraulic
206 conductivity contrast between the background sand and the barrier. The head drop is
207 predominantly dissipated over the background sand upstream of the barrier, resulting in the high
208 head drop over the samples with the finer B15 background sand (M23 and M34, grey lines).

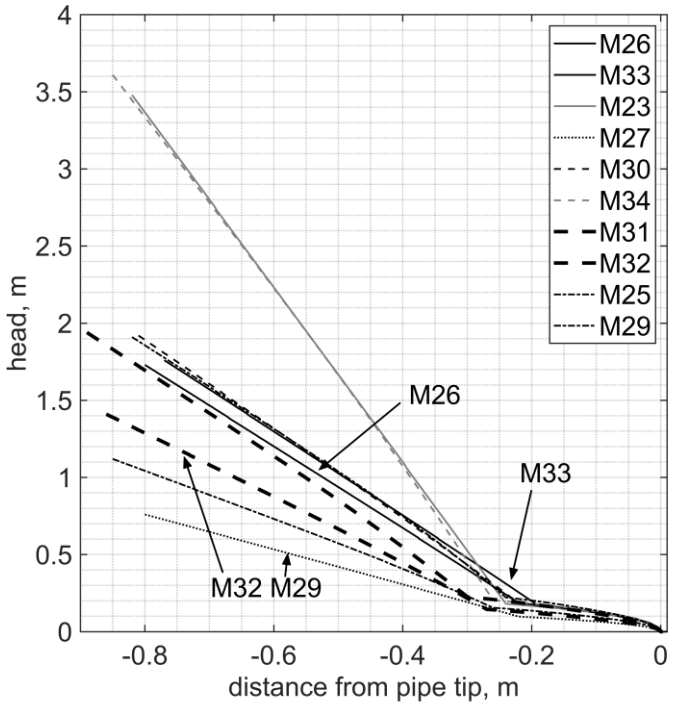

209 *a)*

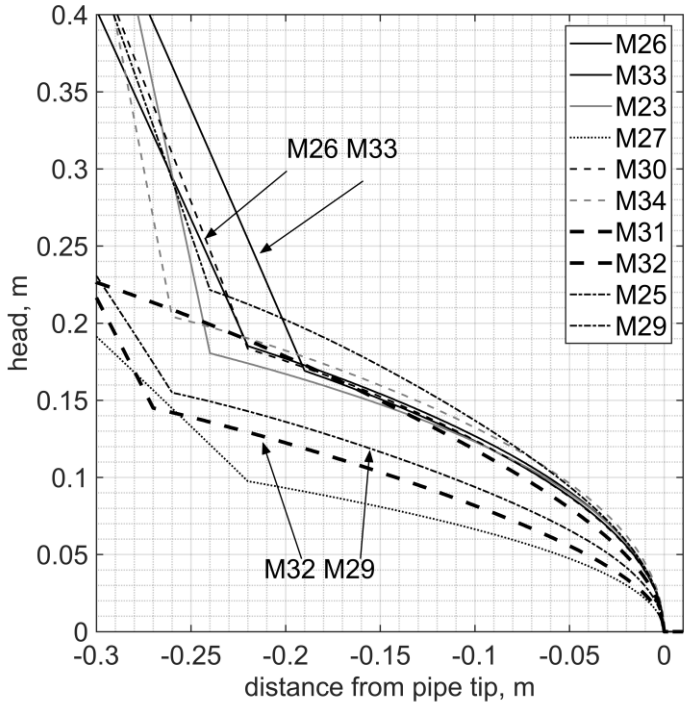

210 *b)*

211 *Figure 4 Modelled head profiles along the upper boundary of the model upstream of the pipe tip*
212 *for tests with GZB1 from the inlet (a), and close-up at the pipe tip (b). Duplicate tests have the*
213 *same line style. Head profiles are referenced to 0.0 m head in the pipe for comparison.*

The head profile curves sharply towards the pipe tip (Figure 4b). This is due to the singularity created by modelling the pipe as a boundary condition with no depth and no head loss in the pipe. In reality, the pipe will have some depth and resistance, and there might be some loosening of grains at the tip of the pipe. Therefore, the modelled head profile in the first 0.02 m upstream of the pipe tip is considered less realistic than the profile in the rest of the model. Head profiles inside the barrier lie closely together for most tests. This would be expected if indeed a local gradient characterises erosion resistance, as the GZB has a similar *RD* in these tests (except in M27 which has a lower *RD*). The head profiles for tests M27, M29 and M32 are lower than for the other tests. M27 has a lower *RD,* therefore a lower head profile is expected. It is unclear why M29 and M32 are lower, duplicate tests (M25 and M31 respectively) have similar head profiles to the other tests, indicating that the difference is not related to the test configuration. Observations during the tests and evaluation of the models in Section 2.2.1 provides no explanation for tests M29 and M32 being outliers, therefore these tests probably reflect variation inherent to the barrier materials. This variation must be considered in determining an appropriate value of the design criterion.

3.2.3 Characterisation of strength criterion

The expectation is that the local horizontal secant gradient over a given distance characterises erosion resistance and can therefore be used as $i_{cp,num}$, however, the calculated vertical and diagonal gradients are also considered. Figure 5 shows the secant gradients in the horizontal, vertical and diagonal direction from the pipe tip over different distances. The computed secant gradients over distances of 0.2 or 0.4 m may overestimate the actual gradients due to the singularity at the pipe tip.

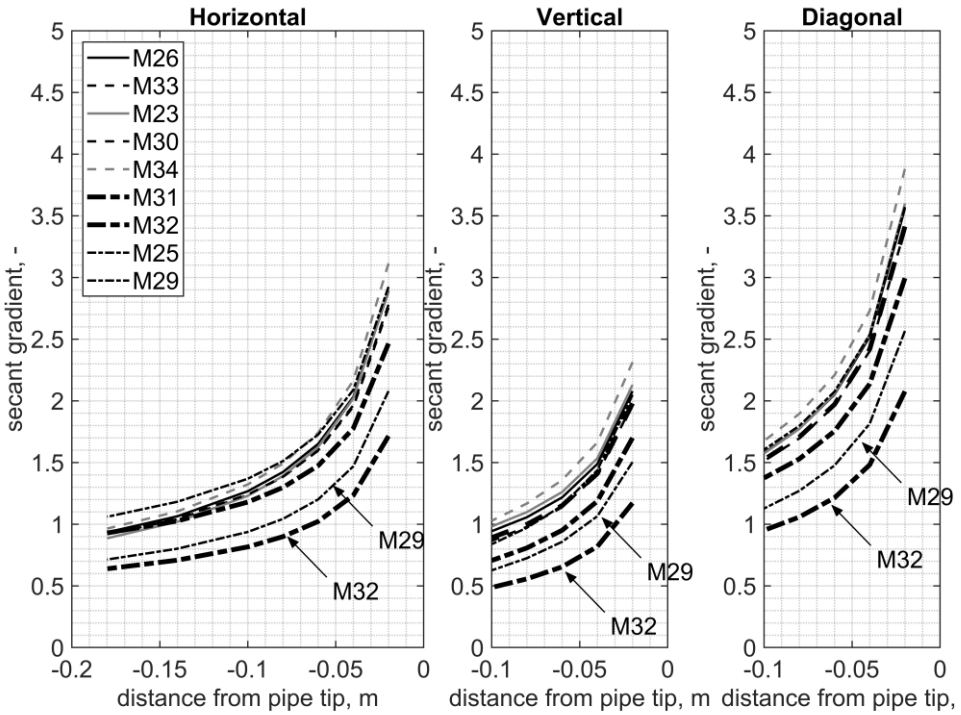

Figure 5: Modelled secant gradients upstream of the pipe tip in the horizontal, vertical and diagonal direction.

The appropriate $i_{cp,num}$ is selected based on the assumption that the modelled gradient at the critical time instant is the same for tests on the same material at the same *RD*. Therefore, the variation among modelled gradients, expressed by the coefficient of variation ($COV = SD/\mu$), is shown for secant gradients for the tests with a dense GZB1 ($RD>0.75$) in Figure 6. Two outliers (M29 and M32) have a large effect on the total variation, as is shown by considering the dataset without those two values. However, there is no reason to reject these test results.

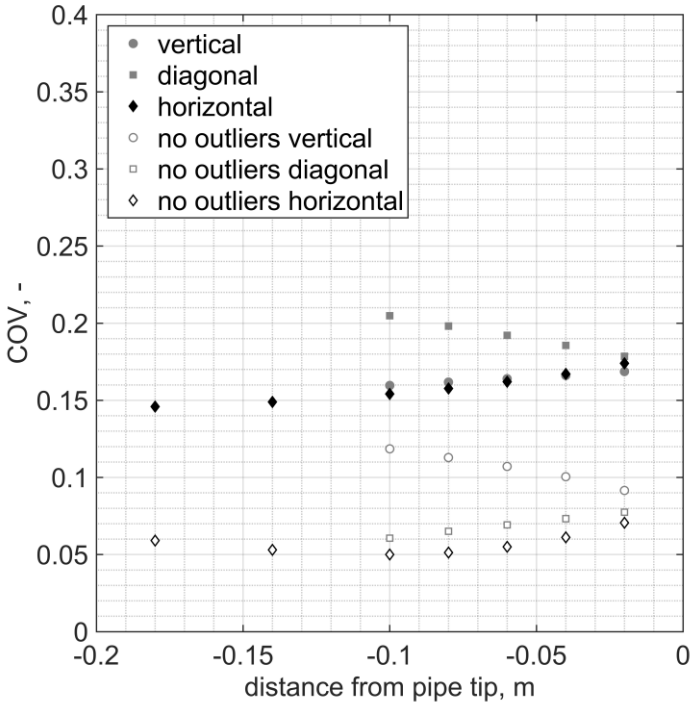

Figure 6: Coefficients of variation (COV = SD/μ) for secant gradients for tests on GZB1 with a high RD.

The horizontal and vertical gradients show a similar amount of variation, which is less than the variation for diagonal gradients. The large number of measurements in the top of the set-up, make the modelled horizontal head profile most reliable, which favours the use of a horizontal criterion. The *COV* of horizontal gradients decreases with increasing distance, which might be due to the relatively larger influence of measurement and model uncertainty on modelled gradients over shorter distances. That might suggest that the gradient over a longer distance is best to characterise the strength criterion, however, from a physical perspective this is less plausible. Pipe progression is considered to be governed by local fluidisation of a group of grains near the pipe tip, and the relevant distance for the criterion is expected to approximately reflect the side of the fluidised group. Probably there was not one unique distance over which the fluidisation occurred in the experiments, as the fluidisation may have been affected by millimetre to centimetre scale variations in the *RD* of the material.

Therefore, the horizontal gradient over 0.10 m is selected as the strength criterion, $i_{cp,num}$, the same distance as used by Robbins et al. (2018). Considering these physical effects, in combination with the numerical uncertainty due to the singularity at the pipe tip and the 3D

nature of the flow field close to the pipe tip, the selected strength criterion should be considered as a practical decision in order to enable modelling of the strength of a CSB.

3.2.4 Effect of RD on $i_{cp,num}$

The measured gradients over the barrier, $i_{cp,exp}$ (Rosenbrand et al., 2020) indicated that the resistance against erosion of the barrier is higher at a higher *RD,* and that the resistance of barriers with a higher C_u (GZB1 C_u 3.7; GZB5 C_u 3.2) is similar, whereas GZB 2 with a lower C_u (2.5) has less resistance. These findings are reflected in the modelled gradients in Figure 7.

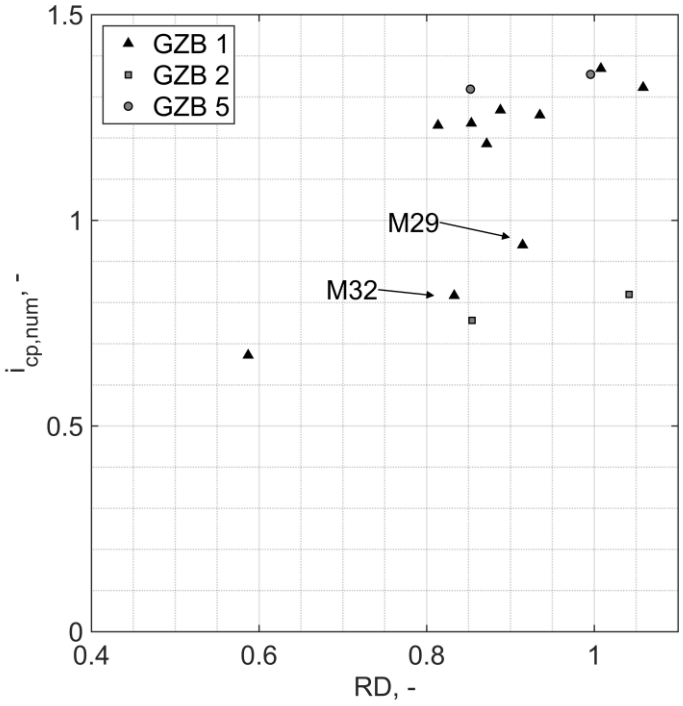

Figure 7: Modelled critical secant gradient $i_{cp,num}$ versus relative density.

The majority of the tests were done on GZB1 with a relatively high *RD*, between 0.79 and 1.07, those tests show some correlation of a higher $i_{cp,num}$ with a higher *RD*. The one test with GZB1 with an *RD* of 0.55 does show a significantly lower $i_{cp,num.}$ as expected. Due to the small variation of *RD* values, and variation that appears to be inherent to the material, no correlation is derived for $i_{cp,num}$ as function of *RD*. For practice, a barrier with a high *RD* is recommended to optimise the strength.

3.2.5 Effect of contrast on critical head drop

The critical head drop, h_{cp}, that can be retained by the barrier is shown a function of the hydraulic conductivity contrast between the barrier and the background sand upstream in Figure

8. The higher the contrast, the larger the portion of the head drop that is dissipated in the background sand (Figure 4). Therefore, a higher critical head drop can be applied before the critical gradient in the barrier, $i_{cp,num}$, is achieved. In the selection of a barrier material, a high contrast is desired, provided that the barrier satisfies the filter rules with respect to the background sand.

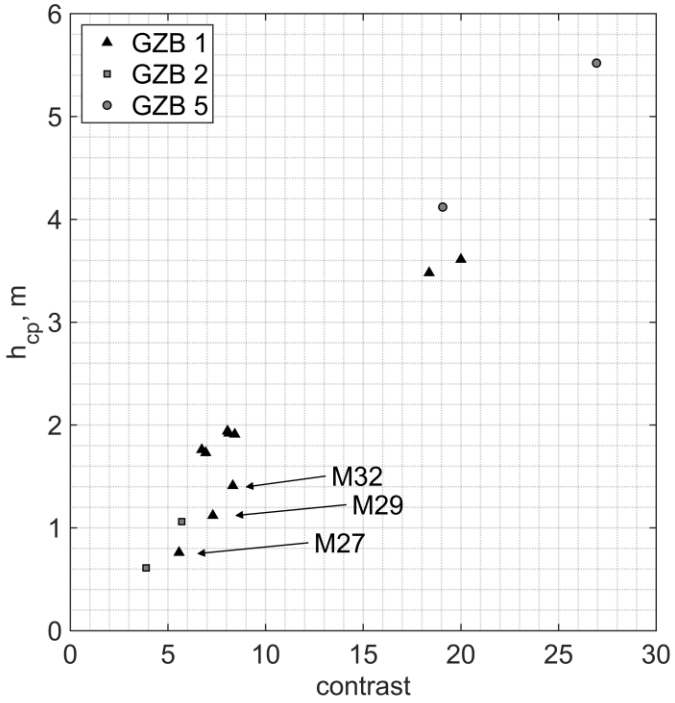

Figure 8: Modelled critical head drop up to the pipe versus hydraulic conductivity contrast.

4 Large-scale experiment: 3D effects

The large-scale experiment (L02) tested the effectiveness of the barrier GZB2. The process of pipe progression was inferred from pore pressure measurements and experience with the medium-scale experiments in Rosenbrand et al. (2020). The pipe appears only to have progressed a limited distance parallel to the interface between the barrier and the background sand; at least 1.2 m, but less than 2.3 m. Therefore, the flow field had a significant 3D component, and both a 2D and a 3D model were used to model this experiment (Rosenbrand and van Beek, in press). Due to convergence of flow from the sides in the 3D model, the head profile was steeper at the pipe tip than in a 2D situation. As the dimensions and location of the pipe could not be directly observed, there were too many variables to fit the 3D model and verify the strength criterion that was derived based on medium-scale tests, as was the original

intention in order to test the hypothesis. The most important finding for field scale application is that the pipe may not always progress parallel to the barrier edge prior to the progression step. This results in the 3D flow situation, and accordingly a higher local gradient at the pipe tip than predicted in a 2D model.

5. Extrapolation to the field scale

Small- and medium-scale experiments showed approximately one order of magnitude increase of the critical head drop could be realised with a barrier (Rosenbrand et al., 2020). However, scale effects are expected to reduce the increase of the critical head drop for the field. Although the strength criterion itself is scale independent, at a larger scale more flow converges to the barrier, reducing the overall critical head drop. Numerical modelling can be used to determine the effect of the barrier for design, as illustrated in this chapter.

5.1 Model description

For practitioners, a design approach using 2D steady state groundwater flow models is envisaged, as 3D models are computationally expensive, complex to construct and require too many assumptions regarding pipe dimensions. Possible 3D effects due to the risk of a pipe not progressing parallel to the entire barrier could be addressed by deriving a correction factor for design.

Models for design would be similar to those used for the medium-scale experiments. For demonstration of the effect of a CSB, a schematisation is made for a case such as might be encountered along the main rivers in the Netherlands. The schematisation, model parameters, and boundary conditions are shown in Figure 9.

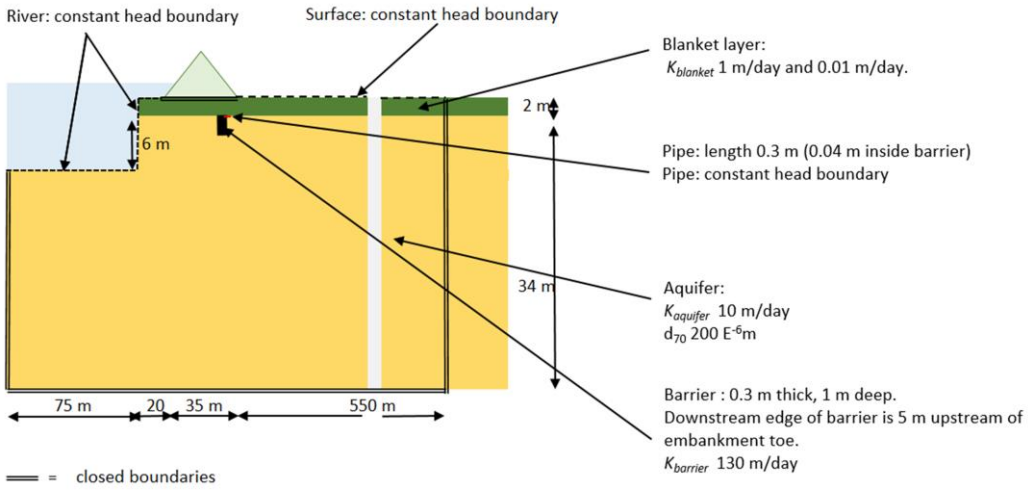

Figure 9: Schematisation of a CSB in a field case. River and embankment are not actually modelled but represented by a constant head boundary (river) and a closed boundary (bottom of embankment). Note barrier and pipe are not to scale.

The left-hand side of the model represents the midpoint of the river, which is a symmetry axis. The CSB is placed in the top of the aquifer just below the cover layer. Steady state groundwater flow is modelled according to Darcy's law. The pipe is modelled just below the blanket layer as a boundary condition with a constant head. This assumes there is zero head loss in the pipe itself. This, conservative, assumption is only applicable for a situation with an effective CSB. Due to the higher head drop that can be retained by the CSB, the pipe downstream of the CSB is larger than a pipe in a uniform aquifer, resulting in less resistance to flow in the larger pipe. For BEP in a uniform aquifer, the head loss in the pipe due to secondary erosion cannot be neglected. Whereas in experiments the length of the pipe in the barrier was observed, for prediction a value has to be estimated a priori. A short pipe length results in a higher modelled gradient, due to flow converging in the barrier to a shorter pipe. The shortest observed length in the medium-scale test is 0.04 m; this conservative value is used to illustrate the effect of a barrier. Whereas in the medium-scale experiments the distance between the outlet hole and the barrier can be modelled entirely as the pipe outflow boundary, this is not representative for the field scale (Rosenbrand and van Beek, in press). A line in a 2D model corresponds to an area in a 3D consideration. For the 2D models of the medium-scale experiments, the approach was appropriate as pipes occupied a significant portion of the area between the outlet hole and the barrier. On the field scale, the width of the pipe relative to the total area covered by the blanket

in front of the barrier is much smaller. Therefore, the pipe downstream of the barrier is only modelled over a distance that represents the pipe that forms parallel to the barrier edge in the background sand. Based on findings from the excavation of one of the large-scale tests, which did not lead to failure of the barrier (Rosenbrand et al., 2019), a length of 0.26 m in front of the barrier is used. To allow for seepage through the blanket layer, the surface of the blanket is modelled by a constant head boundary. The side and bottom boundaries of the model, as well as the length representing the base of the embankment are closed (Figure 8).

For illustration purposes, the strength criterion of the barrier is the average $i_{cp,num}$ for the 9 tests on GZB1 with an RD > 0.75, which is 1.2. For application in practice, a design philosophy is required to determine a design value of the barrier strength based on the required probability of failure. The river head boundary condition is a fictious 1 m, the head in the pipe and at the surface of the blanket in the hinterland are both 0 m. This means that the head drop in the sand boil over the blanket is negligible for this example.

The mesh is locally refined in the barrier to 0.02 m elements, a 5 m zone of refined elements is placed around the barrier from which the element size gradually increases to 20 m at the sides and bottom of the model (S2 Figure S2.1).

The hydraulic conductivity of the natural soil is based on what can be encountered in the river area in the Netherlands, and hydraulic conductivity of the barrier is based on the correlation between RD and GZB1. The hydraulic conductivity contrast between the barrier and the background sand based on the values (shown in Figure 9) is 13. The permeability of the blanket can be highly variable. The effect of the permeability of the blanket is investigated to demonstrate its effect on the concentration of flow to the pipe.

For a head drop of 1 m between the outer water body and the pipe, the model is used to compute the gradient 0.10 m upstream of the pipe tip $i_{1m,num}$. As groundwater flow scales linearly, the ratio $i_{cp,num}/i_{1m,num}$ equals the critical head drop, h_{cp}.

5.2 Results and discussion

The modelled head profiles are shown in Figure 10, these illustrate that the head drop is mainly dissipated upstream of the barrier (head distributions are shown in S2 Figures S2.2 and S2.3). The head profile in the barrier is higher for a less permeable blanket, as there is less leakage to the surface through the blanket, resulting in a higher head in the aquifer close to the barrier.

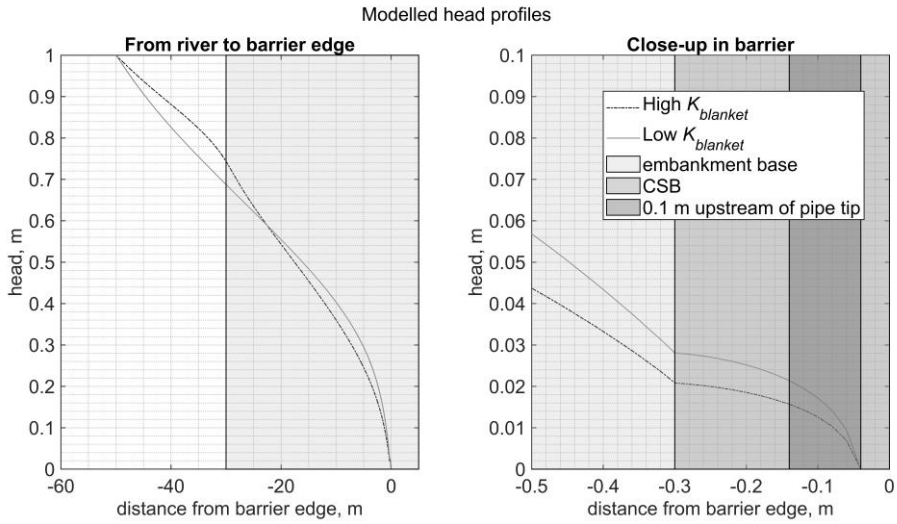

374

375 *Figure 10 Modelled head profiles for field example.*

376 The critical head drops are 10.5 (high $K_{blanket}$) and 7.7 m (low $K_{blanket}$). Using the Sellmeijer
377 calculation rule (Sellmeijer et al., 2011), which used to assess BEP in the Netherlands
378 (Ministerie van Infrastructuur en Milieu, 2017), the critical head drops would be 3.6 (high $K_{blanket}$)
379 or 3.7 m (low $K_{blanket}$) respectively. Thereby the barrier provides a two to threefold increase.
380 Although the effect of $K_{blanket}$ on the critical head drop with a CSB is expected, it is to be noted
381 that this does not play a significant role in the Sellmeijer rule. Thus, a barrier is a particularly
382 promising measure in areas where seepage to the hinterland contributes significantly to
383 dissipation of pore water pressures in the aquifer.
384 For design, a safety philosophy is required in order to account for natural variability in the
385 strength of the barrier material, and the possibility that the pipe progression is incomplete along
386 the barrier resulting in 3D flow. This would presumably result in a lower criterion that can be
387 used for design, and thereby a lower strength gain. Nonetheless, the demonstration shows that
388 despite scale effects, the barrier is a promising reinforcement measure providing a significant
389 increase in critical head drop that can be retained.

390 **6. Conclusions**

391 This paper formed the second step in the investigation of a coarse sand barrier (CSB) as a
392 novel remediation measure against backward erosion piping. The CSB is a trench filled with
393 densified coarse sand or gravel which is placed below the toe of an embankment at the top of
394 the aquifer just below the blanket layer. The first step consisted of analysis of the laboratory
395 experiments at three scales to test the CSB, in Rosenbrand et al. (2020).

In step two, numerical modelling of the laboratory experiments was used to derive a local strength criterion that characterises the resistance of a CSB against BEP. The local strength criterion, which is considered to be independent of scale, can be applied for design by means of numerical modelling. This was illustrated by a field scale example, which illustrates that the CSB increased the critical water level that could be retained by a factor 2-3.

The local strength criterion is a function of the *RD* of the CSB, a high *RD* provides a higher resistance. A higher overall head drop can be retained when the hydraulic conductivity contrast between the barrier and the background sand is higher, which in combination with the location of the CSB can be optimised in design.

For design, a safety philosophy is required to determine a characteristic value for the strength criterion, accounting for natural variability of the material. This philosophy should also account for possible strength reduction due to 3D effects, which might reduce the strength gain in certain circumstances. The next steps in the feasibility study involve application of the CSB at a pilot location in the Netherlands, development of the safety philosophy for design, and assessment of the CSB for situations where the CSB is not level with the aquifer as in the current analysis but protrudes into the cover layer as might occur in certain field situations.

Acknowledgement

The National Flood Protection Programme, and the Water Authority Rivierenland are acknowledged for their support of this investigation. The authors warmly thank the colleagues that contributed their time and expertise to these experiments.

References

Hanses, U. (1985) *Zur Mechanik der Entwicklung von Erosionskanälen in geschichtetem Untergrund unter Stauanlagen.* Dissertation, Grundbauinstitut der Technischen Universität Berlin, Berlin, Germany.

Ministerie van Infrastructuur en Milieu. (2017) Regeling veiligheid primaire waterkeringen 2017. Bjilage III Sterkte en Veiligheid. See https://www.helpdeskwater.nl/onderwerpen/waterveiligheid/primaire/beoordelen/documenten-wbi/?Zoe_Selected_facet:WBI%20gebruiksfunctie=19788

Navin, M. (2016) Kaskaskia Island and Bois Brule Levee Breaches During the 1993 Mississippi River Flood. In *Proceedings of USSD International Symposium on the Mechanics of Internal Erosion for Dams and Levees*.

Negrinelli, G., van Beek, V.M., & Ranzi, R. (2016) Experimental and numerical investigation of backward erosion piping in heterogeneous sands. In *Proceedings of the 8th International Conference on Scour and Erosion.* CRC Press Taylor & Francis Group, London, UK, pp. 473-482.

Robbins, B.A., van Beek, V.M., López-Soto, J.F., Montalvo-Bartolomei, A.M., & Murphy, J. (2018) A novel laboratory test for backward erosion piping. International Journal of Physical Modelling in Geotechnics. **18(5)**: 266-279.

Rosenbrand E., van Beek, V.M., van Esch, J.M., Förster, U., Koelewijn, A.R., Voogt, L., Bezuijen, A., Vandenboer, K., & van Gerven, K. (2018) Investigation of the coarse sand barrier against backward erosion piping. In *Proceedings of the 9th International Conference on Scour and Erosion* (Keh-Chia, Y. (eds)). CRC Press Taylor & Francis Group, London, pp. 91-98.

Rosenbrand E. and van Beek, V.M. (in press) Numerical simulation of a large-scale backward erosion piping experiment in 2D and in 3D. In: *Proceedings of International Conference on Scour and Erosion.* Washington DC, USA, 2020.

Rosenbrand, E., van Beek, V.M., Bezuijen, A., Akrami, S., Terwindt, J., Koelewijn, A.R. & Förster, U. (2020) Multi-scale experiments for a coarse sand barrier against backward erosion piping. Geotechnique published ahead of print https://doi.org/10.1680/jgeot.19.P.358.

Froiio, F., Callari, C., Rotunno, A. (2019) A numerical experiment of backward erosion piping: kinematics and micromechanics. Meccanica. **54(14)**: 2099-2117, https://doi.org/10.1007/s11012-019-01071-7.

Sellmeijer, J.B., Lopéz de la Cruz, J., van Beek, V.M. & Knoeff, J.G. (2011) Fine-tuning of the piping model through small-scale, medium-scale and IJkdijk experiments. European Journal of Environmental and Civil Engineering **15(8):** 1139-1154.

El Shamy, U. and Aydin, F. (2008) Multi-Scale Modeling of Flood-Induced Piping in River Levees. Journal of Geotechnical and Geoenvironmental Engineering, ASCE, **134(9)**:1385-1398.

Schmertmann, J.H. (2000) The no-filter factor of safety against piping through sands. In *Judgement and innovation* (F. Silva and E.J. Kavazanijian (eds)). American Society of Civil Engineers, pp. 65–133.

Van Beek V.M., Knoeff H. & Sellmeijer H. (2011) Observations on the process of backward erosion piping in small-, medium- and full- scale experiments. European Journal of Environmental and Civil Engineering **15(8)**: 1115-1137

Van Beek, V.M., van Essen, H.M., Vandenboer, K., & Bezuijen, A. (2015) Developments in modelling of backward erosion piping. Géotechnique **65(9)**: 740-754.

Van Esch, J.M., Sellmeijer, J.B. & Stolle, D. (2013) "Modeling transient groundwater flow and piping under dikes and dams." In *Proceedings of*. COMGEO III, Krakow, Poland, International Centre for Computational Engineering.

Vrijling, J.K., Kok, M., Calle, E.O.F., Epema, W.G., van der Meer, M.T., van den Berg, P., & Schweckendiek, T. (2010) *Piping: realiteit of rekenfout?*, Report Expertise Netwerk Waterveiligheid, Rijkswaterstaat, The Netherlands. See https://www.enwinfo.nl/images/pdf/Piping-Realiteit-of-Rekenfout-(72dpi).pdf.

Winsemius, H.C., Aerts, J.C.J.H., van Beek, L.P.H., Bierkens, M.F.P., Bouwman, A., Jongman, B., Kwadijk, J.C.J., Ligtvoet, W., Lucas, P.L., van Vuuren, L.D.P., & Ward, P.J. (2016) Global drivers of future river flood risk. Nature climate change. **6**: 381-385.

Yao, Q., Xie, J., Sun, D.J., and Zhao, J. (2009) *Data collection of dike breach cases of China,* Sino-Dutch cooperation project report. Institute of Water Resources and Hydropower Research, Beijing, China.

List of figure captions

List of table captions